Optocoupling in CMOS

V. Agarwal[1], S. Dutta[2], A. J. Annema[1], R. J. E. Hueting[2], J. Schmitz[2], M.-J. Lee[3], E. Charbon[3] and B. Nauta[1]

[1]IC design group, University of Twente, Enschede, The Netherlands. Email: v.agarwal@utwente.nl
[2]MESA+ Institute for Nanotechnology, University of Twente, Enschede, The Netherlands.
[3] Advanced Quantum Architecture Lab (AQUA), EPFL, Neuchâtel, Switzerland.

Abstract— For on-chip data communication with galvanic isolation, a monolithically integrated optocoupler is strongly desired. For this purpose, silicon (Si) avalanche mode LEDs (AMLEDs) offer a great potential. However such AMLEDs have a relatively low internal quantum efficiency (IQE) and high power consumption. For the first time, in this work, data communication in a monolithically integrated optocoupler is experimentally demonstrated. The novelty of this work is the use of highly sensitive single-photon avalanche diodes (SPADs) for photo-detection to compensate for the low IQE of AMLEDs. We investigated our optocoupler realized in a standard 140 nm CMOS SOI technology, without post-processing, for various LED designs and points of operation. The power consumption of the AMLEDs is minimized through a novel AMLED design and employment of a low power LED driver circuit. The advantages of AMLEDs over forward biased Si LEDs are also demonstrated. For the best AMLED design, the achievable data rate is few Mbps and the energy consumption a few nJ/bit. The active area of the proposed systems is < 0.01 mm^2.

I. INTRODUCTION

Many smart power applications require data communication between different voltage domains with galvanic isolation. Currently this is achieved using inductive isolators, capacitive isolators or discrete optocouplers [1]. Such isolators have various disadvantages: they are large in size, source of extra complexity and costly. In addition, some are also sensitive to external interferences. Conversely, when monolithically integrated, optocouplers in standard CMOS technologies are largely free of such issues. Communication by means of light is also attractive because light is robust to external electrical or magnetic interferences.

So far, optocouplers have not been monolithically integrated in standard CMOS because of the poor overlap between the emission spectrum of a (traditional) forward biased Si LED and the responsivity of a Si photodetector (PD) (Fig. 1a). Therefore, in most discrete optocouplers, LEDs are designed using III-V compounds e.g. GaAs [2] and PDs are typically implemented using Si. This heterogeneous integration makes fabrication more complicated and thereby expensive.

In avalanche mode, Si AMLEDs have an emission spectrum in the visible wavelength region [3]; this spectrum has a significant overlap with the responsivity of Si PDs (Fig. 1b). The spectrum of AMLEDs is due to the radiative recombination of high-energy carriers during avalanche breakdown [3]. However, AMLEDs have a poor IQE (~10^{-5}) [4]. Also, systems implemented with AMLEDs can be power hungry because of the avalanche operation under high voltage [4,5].

The significant development of SPADs in CMOS [6] opens new doors for monolithic integration of optocouplers. SPADs are highly sensitive PDs and can be used to compensate for the poor IQE of AMLEDs. SPADs also have a count rate of up to tens of Mbps, which is sufficient for many smart power applications. For the first time, we report the integration of Si AMLEDs-SPADs for optocoupling applications (Fig. 2).

It was shown that the breakdown voltage (V_{BR}) of AMLEDs can be reduced down to 6 V without degrading their IQE [7]. In this work, we have designed novel AMLED structures to reduce their V_{BR} for low power consumption and then we employed these AMLEDs for optocoupling focusing on power consumption, speed and bit-error-rate (BER). The LEDs and SPADs were designed in a 140 nm CMOS SOI technology; the LED driver and SPAD quenching-and-recharge circuits (QRCs) were implemented externally using off-the-shelf components. The proposed optocoupler (LEDs and SPADs) occupy much less area (~ 0.008 mm^2) compared to inductors (~ 1.9 mm^2 in [8]) and capacitors (~ 1.6 mm^2 in [9]) of inductive and capacitive isolators respectively. The LED driver and QRCs can be integrated on-chip at relatively low area requirements [4,6]. The results suggest a great potential of the AMLED-SPAD combination for monolithic optocoupling applications.

II. EXPERIMENTAL DEVICES

A. AMLEDs and SPAD designs

Fig. 3 shows schematic cross-sections of the two LEDs (A1,A2) and the SPAD (S1). A1 is a vertical n+-pwell diode. For optimized light emission with a minimal V_{BR}, A2 was implemented using closely spaced p+-n+ layers in an n-well. To reduce the dark count rate (DCR) of S1, the depletion region was isolated from the shallow trench isolation using a lowly doped guard ring [10]. The galvanic isolation was implemented using medium trench isolation (MTI); the MTI in this technology can provide an isolation of > 100 V [11]. Fig. 4 shows the micrograph of the devices A1-S1 and A2-S1. A "C"-shaped layout of A2 was designed to increase the coupling efficiency between A2 and S1.

Fig. 5 shows the reverse I-V characteristics of the devices. The high leakage current for A2 is most likely because of the presence of band-to-band tunneling. This was verified by the temperature dependence of the V_{BR}. For A2, V_{BR} was practically constant between 0 – 75 °C: possibly because the negative temperature dependency of Zener breakdown counteracts the

positive temperature dependency of avalanche breakdown [12]. Fig. 6 shows the AMLED light emission profiles and spectra.

The DCR of the SPADs were measured using a passive QRC. Fig. 7 shows the dependence of the DCR on the excess bias voltage V_{EX} (the excess voltage at which the SPAD is biased above breakdown) for different temperatures. The inset also shows the DCR measurement setup schematics. Fig. 8 shows the photon detection probability (PDP) of these SPADs, indicating their higher sensitivity in the visible wavelengths.

S1 was biased above breakdown and the avalanche firing rate (AFR) of S1 was measured when the corresponding LED was biased at the same DC current level in avalanche mode (AM) or in forward mode (FM), *i.e.* an FMLED. In dark conditions, AFR is equivalent to DCR. For the AM operation, the measured AFR was ~ 4x higher than that for the FM operation (Fig. 9). Despite that the IQE for an FMLED is about two orders of magnitude higher [13] than that of an AMLED, Fig. 9 demonstrates better spectral overlap for AMLED-SPAD than that for FMLED-SPAD. Fig. 10 shows the DC coupling between the A1-S1 and A2-S1 when S1 was operated as a "conventional" photodiode. A higher coupling efficiency (η_{CE}) is observed for A2-S1 than for A1-S1.

B. LED driver circuit schematics

Fig. 11 describes the equivalent circuit of our LED driver. It is a self-quenched driver circuit that limits the amount of charge-per-bit (Q_b) and energy-per-bit (E_b) through the LED. For more details about this driver circuit, please refer to [4] in which we present a fully integrated version.

C. Data modulation and BER definition

For SPADs, the data are encoded in their timing response [14]. Therefore, an appropriate modulation scheme for data communication using SPADs is a pulse position modulation (PPM) [14]. Fig. 12 shows the schematics of the LED driver control signals IN and RST for this modulation scheme. A PRBS data sequence with a length of 2^{10} bits was generated and the performance of the optical links was measured in response to this data sequence across all LEDs and operating conditions.

The received data is decoded from the timing response of the SPAD: if the SPAD is triggered only during the first half of the bit duration, data bit is demodulated as a "0", and if the SPAD is triggered only during the last half of the bit duration, data bit is demodulated as "1". For all other cases, data cannot be reliably decoded and those cases were counted as bit-error (Note: BER > 0.5 is possible as per this definition). Using the demodulated data, the BER of the link was estimated.

III. OPTICAL LINK PERFORMANCE

Fig. 13 shows an example of the measured transients of the control signals of the driver circuit, I_{AMLED} and output of QRC (V_{OUT}) at the specified operating conditions.

Figs. 14 and 15 show the estimated BER of the system for different operating conditions when the LEDs were operated in FM and AM respectively. Both in AM and FM, A2-S1 show a lower BER than A1-S1 because of the higher η_{CE} (see Fig. 10). At higher f_S, T_{ON} reduces (Fig. 11) and therefore Q_b

decreases [4]; a lower Q_b reduces the amount of photons per bit (P_b) and thereby increases the BER.

In AM, a much lower BER is obtained compared to FM operation. At higher f_S, A2 shows a lower BER also because of its lower resistance (~ 25 Ω) than A1 (~ 850 Ω): for a fixed T_{ON}, a low resistance results in a high Q_b and consequently a high P_b, therefore a low BER [4]. Fig. 16 shows the measured BER of the optical link as the E_b through the LEDs was varied for several f_S in FM and AM. In AM, A2 requires ~ 2x lower E_b than A1 for a similar BER which demonstrates the advantages of our low V_{BR} AMLED design. The bare BER performance measured here can be improved using (e.g. Hamming) error-correction techniques, requiring a limited number of (low voltage) logic gates.

These results demonstrate that SPADs combined with AMLEDs are attractive for monolithically integrated optocouplers. The performance of the system has been measured up to 1 Mbps. The AMLEDs are expected to reach a high modulation speed; 10 Mbps using AMLEDs in this technology was shown in [4]. The designed SPADs in this technology require a deadtime of about 100 ns for a low afterpulsing probability [15]. This would limit the speed of SPADs up to ~ 10 Mbps. Therefore, the maximum expected single channel data rate of the proposed system is ~ 10 Mbps.

IV. CONCLUSIONS

In this work, for the first time, we have successfully demonstrated data communication using a monolithically integrated optical link in a standard CMOS technology without any post processing. The optical link was implemented using Si AMLEDs and SPADs. The advantages of AMLEDs over forward biased Si LEDs were shown. The coupling efficiency of LEDs with Si PDs was improved by a novel AMLED design. Poor quantum efficiency of AMLEDs was compensated by the use of highly sensitive SPADs. The energy consumption of the system was minimized by the design of novel AMLEDs and low power driver circuits. The results show strong potential of AMLEDs-SPADs combination for monolithic optical links.

REFERENCES

[1]. K. Gingerich *et al.*, Appl. Report SLLA198, *Texas Instruments*, 2006.
[2]. IL4208 Optocoupler, Product dataheet, *Vishay Semiconductors*.
[3]. R. Newman, *Phys. Rev.*, **100**(2), 1955.
[4]. V. Agarwal *et al.*, *Opt. Express*, **25**(15), 2017.
[5]. N. Lodha *et al.*, *Proc. IISW*, 2013.
[6]. A. Rochas *et al.*, *Rev. Sci. Instrum.*, **74**(7), 2003.
[7]. S. Dutta *et al.*, *IEEE EDL*, **38**(7), 2017.
[8]. P. Lombardo *et al.*, *IEEE (ISSCC)*, pp. 300-301, 2016.
[9]. Y. Moghe *et al.*, *2012 IEEE SOI Conference*, pp. 1-2, 2012.
[10]. C. Veerappan *et al.*, *IEEE J. Sel. Top. Q. Elec.*, **20**(6), 2016.
[11]. P. Wessels *et al.*, *Solid-state electronics*, **51**(2), 2007.
[12]. S.M. Sze and K. K. Ng, "Physics of semiconductor devices", Wiley, 2007.
[13]. V. Puliyankot *et al.*, *IEEE Trans. Elec. Dev.*, **59**(1), 2012.
[14]. C. Favi *et al.*, *Proc. 45th ACM/IEEE Des. Aut. Conf.*, pp. 343-344, 2008.
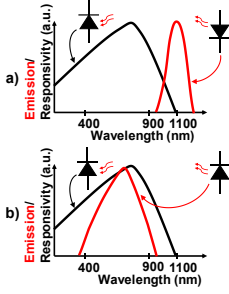[15]. M.-J. Lee *et al.*, *Opt. Express*, **23**(10), 2015.

Fig. 1. Schematic illustration of a relatively (a) poor overlap between the emission spectrum of a forward biased Si LED (FMLED) and the responsivity of a Si PD. (b) good overlap between the emission spectrum of a Si avalanche mode LED (AMLED) and a Si PD. Sketches are derived using [4,7,12].
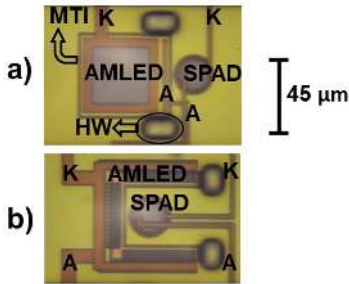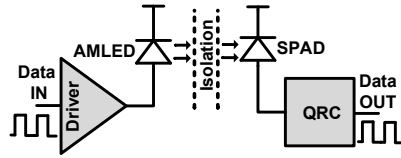

Fig. 2. Proposed optical link comprising of AMLEDs and SPADs. The LED driver circuit drives the LED in response to the incoming data to transmit photons across the isolation barrier. Some of these transmitted photons are detected across the barrier by the SPADs with quenching-and-recharge circuits (QRCs). The data is demodulated from the output of QRCs.
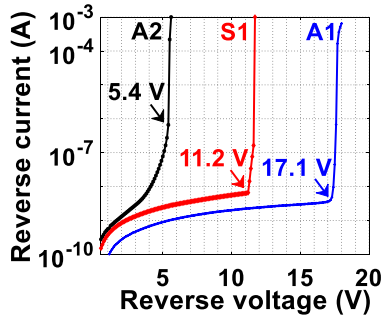

Fig. 3. Schematic cross-section (not to scale) of LEDs (A1, A2) and SPAD (S1); all dimensions in μm. Medium Trench Isolation (MTI) layers provide galvanic isolation between LEDs/SPADs.

Fig. 4. Micrograph of (a) A1-S1 (b) A2-S1. "K" and "A" indicate cathode and anode respectively. Closest distance between the active areas of the LED and the SPAD in both cases is 10 μm. The "C" shaped layout of A2 was chosen to increase coupling efficiency (η_{CE}) between LED and PD (Fig. 10). A circular SPAD is used to reduce edge breakdown. "HW" is handle wafer contact, acting as heat sink.

Fig. 5. Reverse I-V characteristics of the devices measured using an Agilent B2901A with 1 s integration time. V_{BR} (indicated) is defined as the voltage at which I_R starts to sharply increase. V_{BR} for A1 had a temperature coefficient of ~16 mV/K whereas V_{BR} for A2 showed negligible temperature dependency. The temperature coefficient of V_{BR} for S1 was measured to be ~ 8 mV/K.

Fig. 6. (Left) Visible light emission profiles from A1 and A2 (on same scale as Fig. 4). AMLEDs were biased at a constant reverse DC current of 10 mA and the images were captured using a Nikon D3100 camera using 30 s integration time. For A1, light is emitted mostly from the edge closest to the p+ region due to high field and current crowding [4]. For A2, light is emitted from the regions between the n+ and p+ regions, indicating a lateral breakdown. (Right) Normalized emission spectra of the two AMLEDs for two I_R values.

Fig. 7. Measured DCR for S1 (12 μm diameter) as a function of $V_{EX} = (V_{SPAD} - V_{BR})$ for different temperatures. At lower temperatures, DCR is reduced due to reduced thermal generation of dark carriers. Inset depicts the schematic of the measurement setup and illustrative transient waveforms. A passive QRC is used with a quenching resistance (R_Q) of 20 kΩ and V_{CC} = 2 V.
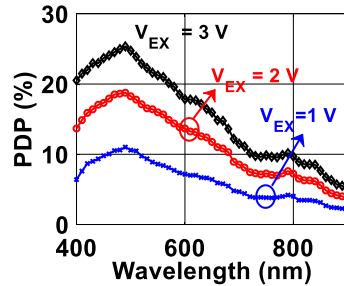

Fig. 8. Photon detection probability (PDP) of SPADs as a function of wavelength of incident photons for different SPAD excess bias [15]. A high sensitivity for photons in the visible spectrum can be observed.
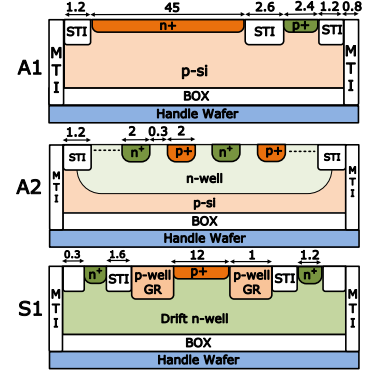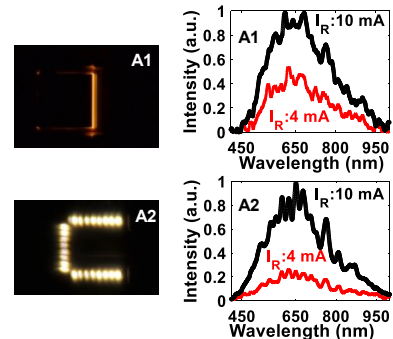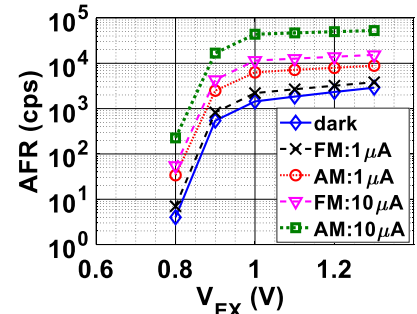

Fig. 9. Avalanche firing rate (AFR) as a function of V_{EX} when S1 was biased above breakdown and illuminated with the integrated Si LED (A1). When A1 was biased using a reverse current in avalanche mode (AM), a higher AFR was obtained compared to the case when A1 was biased using a same value of forward mode (FM) DC current. In dark conditions, AFR is equivalent to DCR.
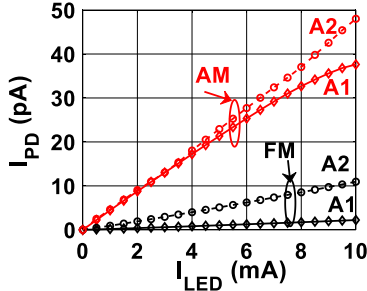
Fig. 10. DC coupling: S1 was operated as a "conventional" PD and its short circuit current (I_{PD}, which is reverse current at $V_R = 0$) was measured when the corresponding LEDs (A1/A2) were biased in AM and FM using DC currents (I_{LED}). A2-S1 shows a higher η_{CE} (= I_{PD}/I_{LED}) than A1-S1 (Fig. 4).
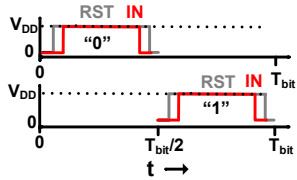

$$V_{EX} \approx V_{AMLED} - V_{BR}$$

$$Q_b \approx \int_0^{T_{ON}} I_{AMLED}(t)\,dt$$

$$Q_b \approx \int_0^{T_{ON}} \frac{V_{EX}(t)}{R_{AMLED}}\,dt$$

$$Q_b \leq C_Q(V_{BIAS} - V_{BR})$$

$$E_b \leq Q_b V_{BIAS}$$

Fig. 11. AMLED driver circuit with illustrative transients [4]. Initially, RST is set high, thus turning off the switch M1. Then IN is set high and initially voltage across an AMLED ($V_{AMLED} = V_{BIAS} - V_{CAP}$) increases to ~ V_{BIAS} (assuming quenching capacitance C_Q >> parasitic capacitance C_{PAR}). As $V_{AMLED} > V_{BR}$, avalanche is triggered and the avalanche current (I_{AMLED}) charges C_Q, thereby increasing V_{CAP} and reducing V_{AMLED}. As V_{AMLED} approaches V_{BR}, the avalanche is quenched. The total charge per bit through the AMLED (Q_b) is limited to $C_Q(V_{BIAS}-V_{BR})$. The energy-per-bit (E_b) is then limited to $Q_b V_{BIAS}$. I_{AMLED} is directly measured on a Keysight DSO-X 3024A oscilloscope. In our setup, Q_b and therefore E_b could be tuned by tuning C_Q and V_{BIAS} (with $V_{BIAS} - V_{DD} < V_{BR}$). A simplified model for an AMLED is shown in the right hand side dashed area [4].

Fig. 12. Illustrative transient waveforms of the control signals IN and RST for bit "0" and for bit "1" when data were modulated using a two-level PPM. $T_{bit} = 1/f_s$ is the bit duration time where f_s is the data rate. For bit "0", photons are transmitted in the first half of T_{bit}, whereas for bit "1", photons are transmitted in second half.

Fig. 13. For A1-S1, $V_{BIAS} = 20$ V, $V_{DD} = 4$ V, $C_Q = 100$ pF, $f_S = 100$ kbps, $V_{EX,SPAD} = 1$ V: (Left) Example of measured transients of the control signals IN and RST (top); measured I_{AMLED} and SPAD QRC output (V_{OUT}) in response to those control signals (bottom). For marked bit 1, SPAD is triggered after some delay whereas SPAD is not triggered for bit 2 causing a bit-error. For bits 3,4,6,7 and 8, SPAD is triggered when AMLED is triggered. For bit 5, SPAD is triggered multiple times. (Right : a zoomed response of I_{AMLED} and V_{OUT} (scales enhanced for clarity)).

Fig. 14. Measured BER vs excess bias of SPAD ($V_{EX,SPAD}$) for different f_S with LEDs (A1,A2) operated in FM (driver circuit of Fig. 11 with cathode and anode of the LEDs interchanged). Operating conditions of the driver circuit: $V_{BIAS} = 4$ V, $V_{DD} = 4$ V and $C_Q = 220$ pF. A2-S1 shows a lower BER because of a higher η_{CE} (Figs. 4 and 10). BER vs E_b is shown in Fig. 16.
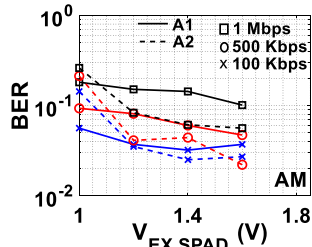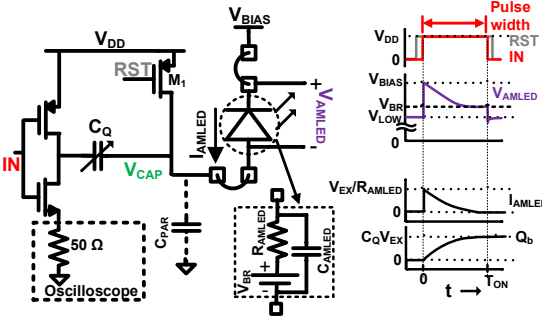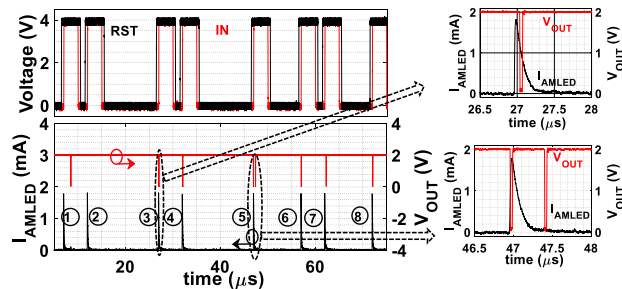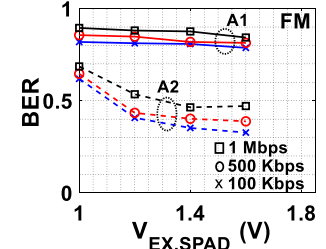

Fig. 15. Measured BER vs $V_{EX,SPAD}$ for different f_S when the LEDs are operated in AM. Note that y-axis is on a different scale than in Fig. 14. Operating conditions of the driver circuit (Fig. 11): $V_{BIAS} = 20$ V for A1 and 9 V for A2, $V_{DD} = 4$ V and $C_Q = 220$ pF. A much lower BER is obtained for AMLED-SPAD combination than for an FMLED-SPAD combination (Fig. 14). BER vs E_b is shown in Fig. 16.
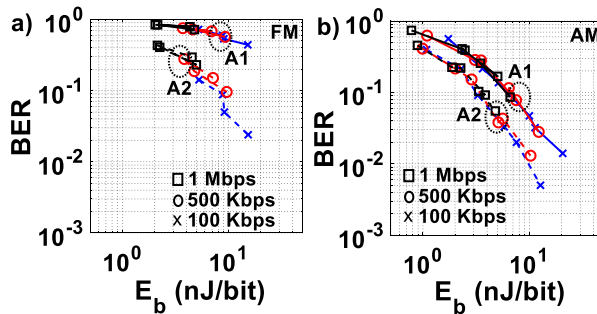

Fig. 16. Measured BER of the optical links as a function of E_b for (a) FM (b) AM LED operation; E_b was varied by varying C_Q and V_{BIAS} for several f_S. For both LEDs (A1,A2), BER reduces for higher E_b because of higher P_b. At similar E_b, A2 shows a lower BER due to a higher Q_b, P_b and η_{CE}. Similar BER were measured across all data rates for similar E_b. $V_{EX,SPAD} = 1.2$ V for all measurements.
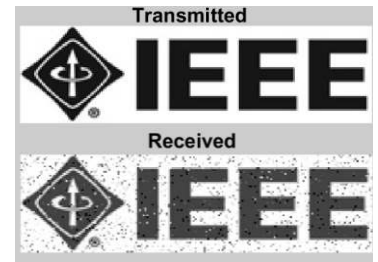

Fig. 17. Application example: IEEE logo (8-bit resolution) transmitted through our optical link A1-S1 (in AM) at 1 Mbps. From the received bits, image was reconstructed without any error-correction. Bits which could not be resolved from SPAD output were estimated as 0 or 1 randomly using uniform distribution.